*Desalination and Water Treatment*
www.deswater.com

doi: 10.5004/dwt.2017.20232

65 (2017) 451–462
February

# Photocatalytic degradation of tetrabromobisphenol A with a combined UV/$TiO_2$/$H_2O_2$ process

Xingxing Peng[a,b], Wanying Li[a,b], Jiejing Chen[a,b], Xiaoshan Jia[a,b,*]

[a]*School of Environmental Science and Engineering, Sun Yat-sen University, Guangzhou 510275, China, Tel. +86-20-39953107; email: eesjxs@mail.sysu.edu.cn (X. Jia)*
[b]*Guangdong Provincial Key Laboratory of Environmental Pollution Control and Remediation Technology, Guangzhou 510006, China*

Received 7 June 2016; Accepted 15 September 2016

**ABSTRACT**

The photocatalytic process of $TiO_2$/$H_2O_2$/UV, first, was applied to degrade tetrabromobisphenol A (TBBPA) in aqueous system. Under the optimal conditions, the degrading efficiency of TBBPA reached 99.3% after 150 min when 120 W UV (0.42 mW/cm$^2$), 3% $H_2O_2$, and 400 mg/L of 500°C-calcined $TiO_2$. During the photocatalytic degradation process, hydroxyl radicals (·OH) were considered to be the main reactive oxidative species involved in attacking TBBPA, and bromide ions generation with the conducting reaction. Moreover, five intermediates were detected by liquid chromatography–mass spectrometry, and a photocatalytic degradation pathway was proposed. The combination with excellent efficiency for TBBPA provided a potential technology for the treatment of TBBPA-contaminated wastewater or environments.

*Keywords:* Tetrabromobisphenol A; UV/$TiO_2$/$H_2O_2$ processes; Photocatalytic degradation; Pathway

## 1. Introduction

Brominated flame retardants (BFRs), for the purpose of fire prevention, are widely used in epoxy resins, polyester resins, phenolic resins, and polycarbonate products (as reactive flame retardants), and they are present in styrene plastics, polypropylene, and polyethylene terephthalate as additive flame retardants among other materials [1]. Because of good thermal stability and largest BFR in terms of production, tetrabromobisphenol A (TBBPA) has drawn a lot of attentions of researchers throughout the world. It has been widely detected in the water, sediment, sewage sludge, landfill leachate, and atmosphere in vivo [2,3]. Toxicology test showed that TBBPA harmed to aquatic animals and plants, such as algae and fish, exhibits definite toxicities [4,5]. With the widespread use of TBBPA and its negative impact on human health, the sources and transformation effecting on humans cannot be ignored. The main toxicity manifests are liver and kidney toxicity [6–8], cytotoxicity [9,10], immune system toxicity [11], nervous system toxicity [12,13], endocrine toxicity [14,15], and so on. Due to the similarity in structure between TBBPA and thyroxine (thyroxin, T4), more and more scholars believe that TBBPA is a potential endocrine disruptor [2,16].

Considering the stable structure of TBBPA, conventional treatment methods are not effective. Current studies on TBBPA mainly focus on physical adsorption, pyrolysis, oxidation degradation, microbial degradation, and advanced oxidative degradation. They are adsorbed through humic acid, tidal soil, and other adsorption mechanisms. Their microbial degradation includes aerobic degradation, anaerobic biodegradation, and aerobic–anaerobic degradation, in which the microbial species are mainly bacteria and fungi. The pyrolysis degradation methods mainly include ZnO pyrolysis [17,18] and $Sb_2O_3$ pyrolysis [19] in a supercritical hydrothermal solution. The oxidative degradation materials include ZnO, PbO, $Cu_2O$ [20], photodegradation [21], $MnO_2$ oxidation [22], and so on. The most common methods used in oxidative degradation are UV degradation, microwave-assisted degradation, ultrasonic degradation, ozone degradation, and photocatalytic degradation.

* Corresponding author.

$TiO_2$ is a stable and non-toxic photocatalyst that exhibits a strong degradation as a photocatalyst for a variety of persistent contaminants, as well as has great potential to contaminant management. It is widely believed that the degradation mechanism of $TiO_2$ is governed by the theory of direct hole oxidation. The electron–hole band mechanism is based on the crystal structure of the material. Anatase $TiO_2$ has a band gap of 3.2 eV under UV excitation. When the photon irradiation energy is higher than the band gap energy, the valence band electrons absorb the photon energy and transition to the conduction band to form a hole in the conduction band, leaving a positively charged valence band. This hole is then filled with an electron again through oxidation. However, the oxidative properties of $TiO_2$ are not internally derived. Ultraviolet irradiation in contact with a $TiO_2$ suspension causes an electron/hole pair to migrate to the surface of the $TiO_2$ particles. The $TiO_2$ particle surface comes in contact with $O_2$, $H_2O$, $H_2O_2$, and other electron acceptors that can accept light generated electrons through adsorption. This causes a redox reaction to occur, with $H_2O$ and other particles around the electron acceptor forming a hydroxyl radical (·OH). The $TiO_2$ surface holes and hydroxyl radical act as a strong oxidant that can degrade organic materials adsorbed on the $TiO_2$ surface. Prior to using $TiO_2$ as a catalyst, it is necessary to prepare nanoscale $TiO_2$. Various methods for preparing nanotitanium dioxide are divided into physical and chemical methods, physical methods including plasma and mechanical crushing method; chemical methods including hydrothermal method [23], microemulsion method, homogeneous precipitation [24], and sol–gel method [25–27]. During the process of preparing nanoscale $TiO_2$, calcination at each stage can lead to grain growth and aggregate formation, so each stage should be strictly controlled [25]. In addition, the manufacturing process produces sulphate ions (ammonium sulphate-based) that are adsorbed on the $TiO_2$ surface and inside pores, impeding contact with the reactants at the surface, thereby reducing the activity of the reaction. Considering sulphate is one of the main factor inhibiting the activity of nanosized $TiO_2$, the content of sulphate should be controlled in nanoscale $TiO_2$ production. Sulphate present in a process using nano-$TiO_2$ catalysts is most likely to be in the form of sulphate ions. Therefore, it is important to explore the role of sulphate ions in the degradation of TBBPA using nano-$TiO_2$ [28].

In this study, a sol–gel method was used to prepare $TiO_2$, which was then calcined at eight different temperatures: 200°C, 300°C, 400°C, 500°C, 600°C, 700°C, 800°C, and 900°C. The physical properties of the $TiO_2$ catalyst were characterized using X-ray diffraction (XRD). As well known, the major deficiencies of the $TiO_2$ based on photocatalytic technology are fast electron/hole recombination and relatively low quantum yields. Therefore, this work attempted to improve the deficiencies through the addition of $H_2O_2$ and to explore the optimal reaction conditions in a $TiO_2/H_2O_2$/UV combined process. Moreover, optimal condition was determined by series experiments containing $H_2O_2$ (1.5%–6.0%) and prepared $TiO_2$ concentration ranged from 100 to 500 mg/L under UV (40–120 W) irradiation. Finally, we investigated the transformation of hydroxyl radicals, analyzed the generation of bromide ions, degrading products during reaction process, then derived the degradation pathways of TBBPA. The purpose of this study was to try to develop new and effective $TiO_2$ photocatalytic technologies to manage TBBPA.

## 2. Materials and methods

### 2.1. Chemicals

TBBPA (99% purity) was purchased from Sigma Chemical Co. (St Louis, MO, USA) and considered to be the target compound. TBBPA was dissolved in acetone to create a stock solution (100,000 mg/L), followed by membrane filtration to remove impurities. It was then diluted into the medium to obtain desired concentrations. All of the solvents (including acetone and methanol) used in this study were high-performance liquid chromatography (HPLC) grade and were purchased from Merck Company (Darmstadt, Germany). Other chemicals used for the medium were of analytical grade and purchased from Sigma Chemical Co. (St Louis, MO, USA). High quality water was prepared using a Nanopure UV deionization system, Barnstead/Thermolyne Co. (Dubuque, IA, USA).

### 2.2. Preparation and characterization of nano-$TiO_2$

In this study, the sol–gel method was used to prepare $TiO_2$ powder. The prepared powder exhibited uniform distribution, good dispersion, and high purity, and the solvent was easily removed at a later stage in the calcination process to reduce impurities in the samples. The preparation process is as follows: 17 mL of tetrabutyl titanate was added to 40 mL of absolute ethanol then stirred rapidly to form a homogenous solution (solution 1); 10 mL of anhydrous acetic acid and 5 mL of distilled water was added to 40 mL of absolute ethanol (solution 2) with a stir bar and placed on a magnetic stirrer; the solution was transferred to a separatory funnel and added dropwise with stirring to solution 2, and stirring continuously for 2 h. The liquid dropped approximately 1 drop per second; after the addition, the solution was allowed to stand at room temperature to allow the gel to form, followed by drying in an oven at approximately 105°C. The dry gel was ground with a mortar into a powder. Next, the powders were calcined for 3 h using a muffle furnace at 200°C, 300°C, 400°C, 500°C, 600°C, 700°C, 800°C, and 900°C, respectively. XRD (Rigaku D MAX 2200 VPC) was used to characterize the eight $TiO_2$ powders obtained at different calcining temperatures. The XRD patterns were used (Cu K$\alpha$ radiation) at a scanning voltage of 30 kV, a current of 30 mA, a scanning angle of 10°–80° 2$\theta$ with a step size of 0.04° 2$\theta$, and a scanning rate of 1°/min. The morphology and structural properties were analyzed by scanning electron microscopy (SEM, Merlin, Zeiss, Germany).

### 2.3. Batch experiment design

Several series of batch experiments were conducted with the nano-$TiO_2$ powders describe above. The $TiO_2$ concentrations of the first round of preparations for the 500°C- and 900°C-calcined powders were 200 mg/L. The initial concentration of TBBPA was 10 mg/L, and the ultraviolet lamp power was 40 W. The series of experiments was designed to explore the impact of different conditions ($TiO_2$ concentration, UV-lamp intensity, and $H_2O_2$ concentration) on the

nano-$TiO_2$ degradation of TBBPA. Experimental process was as follows: the concentrations of the reaction catalyst (500°C- and 900°C-calcined $TiO_2$ powders) were 200, 300, 400, and 500 mg/L, respectively; the initial concentration of TBBPA was 10 mg/L; the ultraviolet lamp power were 40, 80, and 120 W, respectively. The intensities of UV lamp 40, 80, and 120 W reaching the reactor solution were 0.28, 0.38, and 0.42 mW/cm$^2$, respectively. Hydrogen peroxide (1.5%, 3%, 4.5%, and 6%) was added to the 500°C- and 900°C-calcined $TiO_2$ reaction systems, respectively. Sulphate catalyst under two conditions (anhydrous sodium sulphate) content was: 0.1, 0.5, 1.0, 1.5, and 2.0 mg/L. All samples firstly were stirred in the dark for 30 min to allow for uniform contact between the catalyst and the contaminant. The UV lamp was turned on to start the reaction, and a sample was taken every 30 min within 150 min. Finally, all samples were filtered through a 0.22 μm membrane into the HPLC for quantitative detection of the TBBPA. In all experiments, the reaction vessel is treated in a four-step process to avoid contamination by first washing in an acidic solution, immersing in an ultrasonicator, cleaning with distilled water, and drying.

### 2.4. Detection of TBBPA

After filtration through the 0.22 μm filters (Merck, Germany), the TBBPA was analyzed with a HPLC (Shimadzu LC-20AT, Kyoto, Japan) equipped with a photodiode array detector (SPD-M20AV) and a VP-ODS column (150 × 4.6 mm, 5 μm). The column was operated at 35°C. A mixture of water and methanol (20:80) at a flow rate of 0.8 mL/min was used as the mobile phase in an isocratic elution mode. The injection volume was 20 μL for all of the solutions, and the detection was performed at a wavelength of 209 nm.

### 2.5. Generation of 2,5-dihydroxy benzoic acid (·OH)

The hydroxyl radical (·OH) is the core of the photocatalytic reaction and acts as an oxidizing agent to produce a radical TBBPA after $TiO_2/H_2O_2$ by UV irradiation. The degradation rate directly affects the level of its production, and the process of measuring the reaction-generated ·OH concentration is particularly important. In this paper, a salicylic acid (2-hydroxybenzoic acid) scavenger was used to indirectly measure the hydroxyl radicals by detecting the produced 2,5-dihydroxy benzoic acid (2,5-DHBA). The reaction mechanism is given as follows:

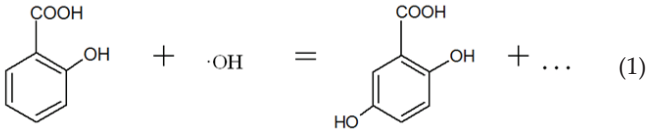


(1)

To obtain the transformation of hydroxyl radical, a 500°C-calcined $TiO_2$ suspension at a concentration of 400 mg/L was prepared with an initial concentration of salicylic acid of 1 mmol/L; the UV lamp power was 120 W, the content of hydrogen peroxide was 3%, the mobile phase acetic acid–sodium acetate was a concentration of 50 mmol/L, and the pH was adjusted to 4.9. Next, it was placed on a magnetic stirrer, and the sample was stirred in the dark for 30 min. The UV lamp was turned on to start the reaction, and the samples were taken at time intervals of 15, 30, 45, 60, 75, 90, and 105 min. Last, the samples were filtered through a 0.22 μm membrane into a HPLC for quantitative detection.

### 2.6. Generation of bromide iron ($Br^-$)

$TiO_2$ was prepared from the 500°C-calcined powder at a concentration of 400 mg/L. The initial concentration of TBBPA was 10 mg/L, and the ultraviolet lamp power was 120 W. 3% hydrogen peroxide was added. The eluent was made from a solution of sodium carbonate, ultrapure water, and sulphuric acid. The samples were left in natural light and stirred for 30 min until the catalyst was uniformly dispersed in the solution to be sure of uniform degradation in the sample. The UV lamp was turned on to start the reaction, and samples were taken every 30 min. The bromide was analyzed by using an ion chromatography (IC) with the model of 733 (Metrohm, Herisau, Switzerland).

### 2.7. Degradation pathway

Because of the excellent analytical qualities of liquid chromatography–mass spectrometry (LC–MS), it is widely used for qualitative studies of material characteristics. This article uses the LC–MS to analyze the degradation products of TBBPA for qualitative purposes, to further analyze its characteristics and the degradation mechanisms, and to derive the TBBPA degradation pathways using the mass spectrograms of the degradation products of TBBPA.

We measured $TiO_2/H_2O_2$ TBBPA degradation during the reaction in the reactor at 10, 20, 30, 45, 60, 90, 120, and 150 min to detect the $Br^-$ and degradation products. The bromide was analyzed by using an IC with the model of 733 (Metrohm, Herisau, Switzerland). Samples for degradation detection were extracted by chloroform and *n*-hexane (1:1). After purification and dried by liquid nitrogen, the remains were dissolved in acetone. The injection volume was 20 L. The procedure was performed on an Agilent 1100 HPLC coupled to an Agilent 6120 quadrupole mass spectrometer (MS) equipped with Zorbax Eclipse XDB C18 column (150 mm × 2.1 mm, 5 μm particle size) with the temperature of 35°C, using 90:10 mixture of methanol (phase A) and water (phase B) as mobile phase at a flow rate of 0.2 mL/min. MS detection performed on a triple quadrupole analyzer equipped with an electrospray ionization source in the negative ion mode.

## 3. Results and discussion

### 3.1. Characterization of nano-$TiO_2$

In this study, the sol–gel method was used to produce different nano-$TiO_2$ powders at different temperatures, and the powders were characterized by SEM (Fig. S1) and XRD (Fig. 1). As seen, from Fig. 1, for samples calcined at temperatures ranging from 200°C to 600°C, $TiO_2$ anatase was the dominant structure in the resulting powders; at a calcination temperature of 700°C, the resulting $TiO_2$ powder was a mixed crystalline phase of anatase and rutile; at 800°C and 900°C, complete conversion to rutile was detected. The two crystalline $TiO_2$ phases of anatase and rutile can be seen

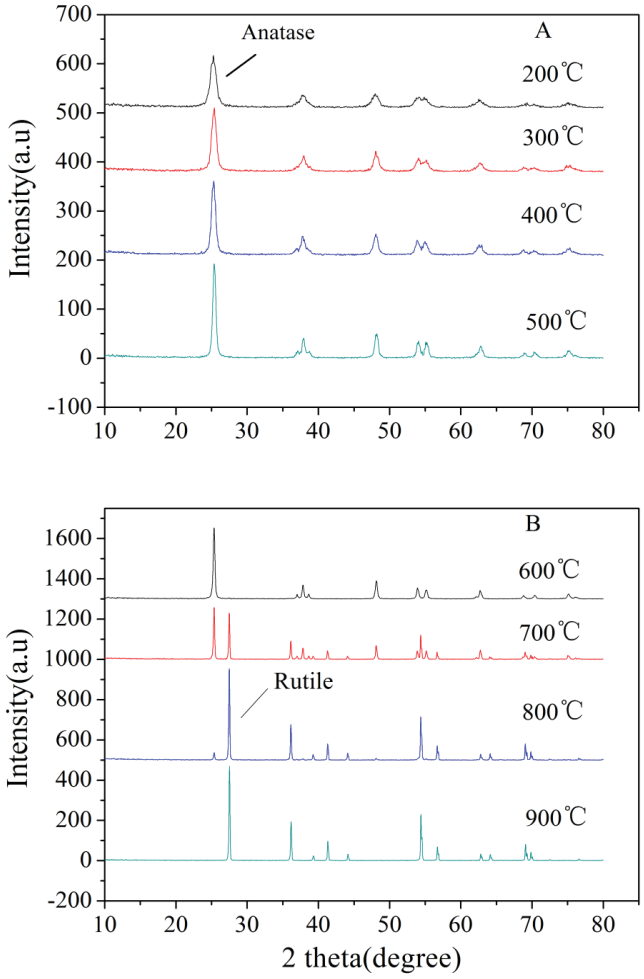


Fig. 1. XRD patterns of nano-$TiO_2$ prepared using the sol–gel method and then calcining at different temperatures (A and B).

from the above XRD, in which the 500°C-calcined samples are mainly anatase $TiO_2$; at 700°C, a mixed crystal form is present. $TiO_2$-calcined at 900°C is mainly rutile. Generally, anatase has a greater photocatalytic activity than rutile [29]. Because the rutile structure has a smaller band gap energy than anatase (rutile phase 3.0 eV and anatase 3.2 eV), it hindered the oxygen reduction reaction in the anatase phase. The crystal lattice has more defects and forms a dislocation network, resulting in more oxygen vacancies that can capture electrons. The rutile phase is the most stable form of $TiO_2$, with a better crystallization state; there are fewer structural defects to trap electrons, thereby accelerating the surface electron–hole pair recombination rate, reducing its photocatalytic activity. The anatase crystal plane (010) in the degradation of some organic materials (such as cyclohexane) has a symmetrical structure allowing for the effective absorption of organic materials. In the heat-treatment process resulting in the anatase to rutile transformation, a sharp irreversible dehydroxylation reaction occurs at the surface of $TiO_2$ occurs, and the surface hydroxyl groups of trapped holes are required to generate hydroxyl radicals and absorb oxygen (to capture electrons) and organics.

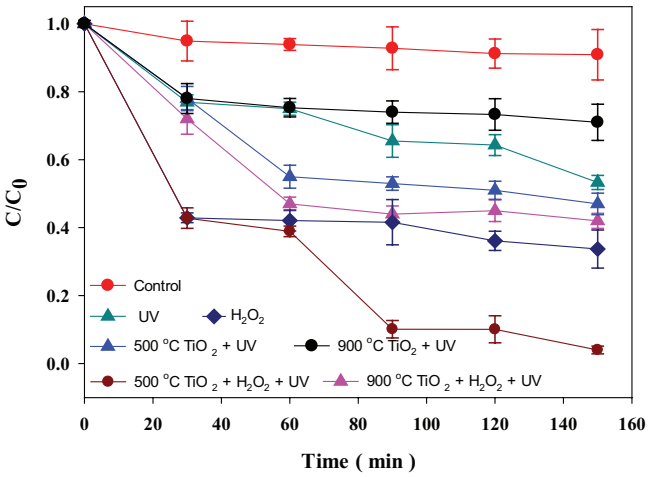


Fig. 2. Comparison of removal capability of 10 mg/L TBBPA at different conditions. Addition of TBBPA to aqueous system: without treatment (control); under UV irradiation (40 W); addition of $H_2O_2$ (1.5%); catalyzed by 500°C- and 900°C-calcined $TiO_2$ under UV irradiation (200 mg/L; 40 W); treated by combination of UV/$TiO_2$/$H_2O_2$ processes (200 mg/L 500°C-calcined $TiO_2$; 40 W; 1.5%); treated by combination of UV/$TiO_2$/$H_2O_2$ processes (200 mg/L 900°C-calcined $TiO_2$; 40 W; 1.5%).

### *3.2. Degradation of TBBPA by the combination of UV/$TiO_2$/$H_2O_2$ processes*

From the earlier test, we selected two typical crystalline forms catalyzed by UV, namely, 500°C- and 900°C-calcined $TiO_2$, respectively, to test the effects on TBBPA degradation. After 150 min treatment, the degradation efficiencies of 500°C- and 900°C-calcined $TiO_2$ were 46.7% and 29%, respectively. Compared with the control, which showed that there is nearly no degradation of 10 mg/L TBBPA (9.1% after 150 min) without any treatment in aqueous system, while treatment catalyzed by $TiO_2$ demonstrated significantly better degradation capacity. Only UV irradiation, addition of $H_2O_2$, and catalyzed by $TiO_2$ under UV, TBBPA degradation efficiencies were enhanced in different extent (Fig. 2). After the addition of hydrogen peroxide to 500°C-calcined $TiO_2$, the catalyst performance rate improved significantly compared with the control (degradation efficiencies of TBBPA increased from 9.1% to 96%). The reaction proceeded for 90 min and tended to be stable, and the sample TBBPA was completely degraded, with a degradation rate as high as 91.9% (Fig. 2). For $TiO_2$-calcined at 900°C treatment with the addition of hydrogen peroxide, the degradation rate was slow, showing that the process was inhibited.

In general, the degradation efficiency addition of $TiO_2$-calcined at 500°C was consistently better than $TiO_2$-calcined at 900°C including different condition of $TiO_2$ concentration, UV-lamp intensity, and addition concentration of $H_2O_2$ (Fig. 3). The degradation efficiency of 400 mg/L $TiO_2$-calcined at 500°C was better than other addition concentration (including 200, 300, and 500 mg/L). It may be because of low $TiO_2$ concentration (200 and 300 mg/L) possessed lower specific surface area, and high concentration protect UV irradiation decreased the TBBPA degradation efficiency [30]. With the UV-lamp intensity increased, the TBBPA degradation efficiency sharply increased (120 W > 80 W > 40 W). In the

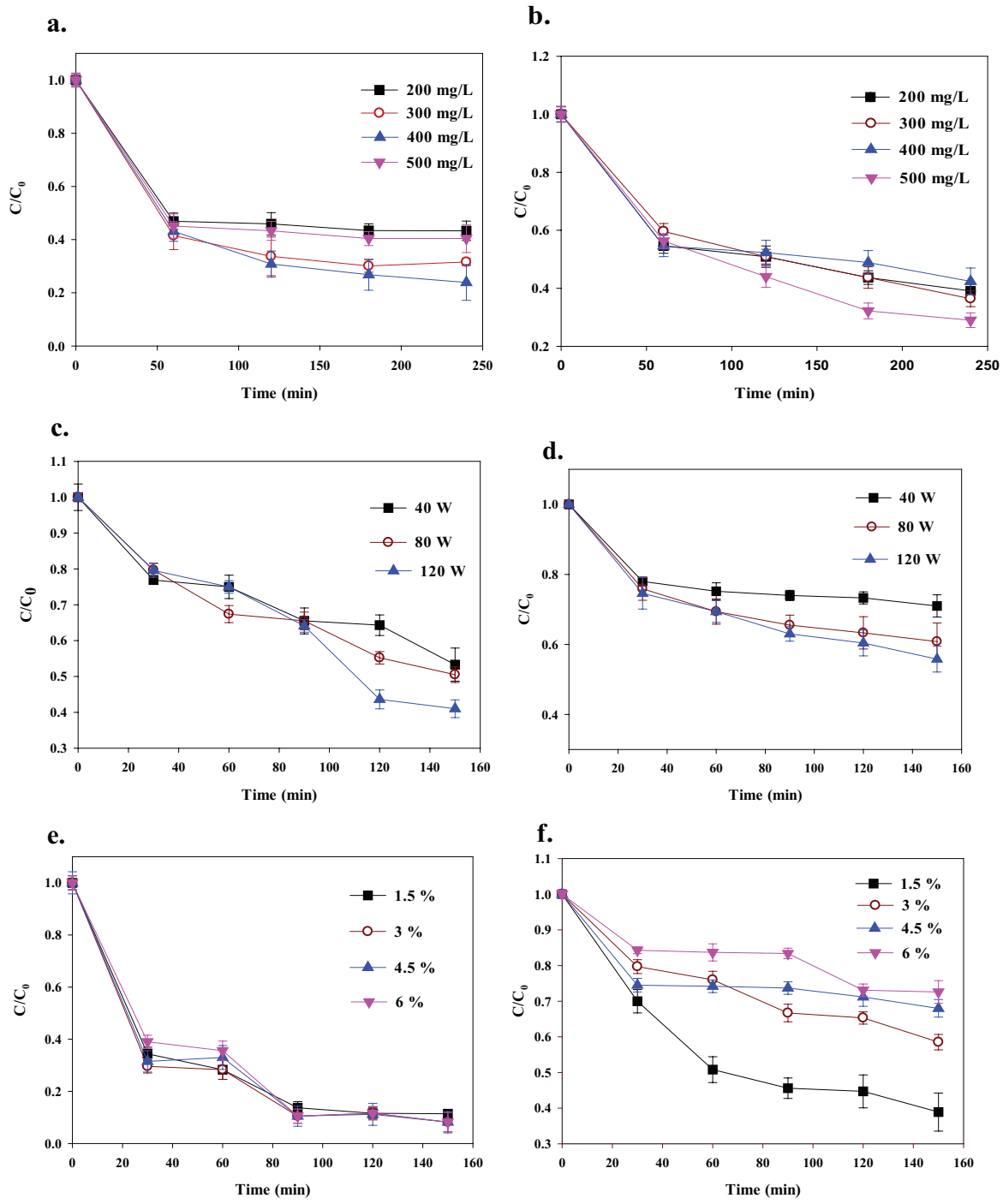


Fig. 3. Degradation of TBBPA by UV/$TiO_2$/$H_2O_2$ process under different combination ((a) 500°C-calcined $TiO_2$ with different concentrations of $TiO_2$; (b) 900°C-calcined $TiO_2$ with different concentrations of $TiO_2$; (c) 500°C-calcined $TiO_2$ with different intensity of UV lamp; (d) 900°C-calcined $TiO_2$ with different concentrations of intensity of UV lamp; (e) 500°C-calcined $TiO_2$ with different concentrations of $H_2O_2$; (f) 900°C-calcined $TiO_2$ with different concentrations of $H_2O_2$).

presence of a hydrogen peroxide content of 1.5%, the degradation rate was 61.1%, which was higher than the other three for $TiO_2$-calcined at 900°C. After increasing the concentration of hydrogen peroxide, $TiO_2$-calcined 900°C for TBBPA degradation was inhibited, and the differences in the degradation curve are significant, showing an overall flat curve as the content of hydrogen peroxide increased. The decreasing trend of the hydrogen peroxide degradation efficiency is presented in Fig. 3(f). After performing the calculation to determine the maximum degradation rate of TBBPA from the different $H_2O_2$

concentrations using the two different crystal forms of nano-$TiO_2$, we find that the $H_2O_2$/UV degradation efficiencies of TBBPA increase initially, then gradually decreases as the process continues. This may be because a certain amount of $H_2O_2$ can act as an electron acceptor to produce electrons in photocatalysis, prompting the reaction to produce a higher volume of hydroxyl radicals (·OH). However, when adding an excess of $H_2O_2$, this may decrease the available light causing the efficiency to decline slightly. The reason for this decline may be that excess of $H_2O_2$ will become an ·OH quencher at the consumption point during the reaction. The ·OH in the photocatalytic reaction is a key oxidant, and reducing the amount of ·OH has a direct effect on the degradation process, resulting in a decreased degradation rate [31]. Based on the results above, it could be concluded that the optimal conditions are 400 mg/L $TiO_2$-calcined at 500°C addition of 3% $H_2O_2$ irradiated by 120 W UV lamp. In the verification experiment, initial TBBPA concentration of 10 mg/L was degraded 99.3% after 150 min under these conditions.

Sulphate ion effect on the degrading process catalyzed by the $TiO_2$ [28]. It may be that a certain concentration of sulphate ions in the solution make it possible to change the settling properties of the catalyst $TiO_2$ and can reduce its agglomeration or coagulation effect, allowing it to remain suspended in the solution and increasing the degradation efficiency (Fig. S2). The main reason for this is that when the concentration of sulphate reaches a saturation point, it may have adsorbed to the $TiO_2$ powder surface and pores, affecting and hindering the $TiO_2$ adsorption contact with TBBPA and even reducing the chance that the TBBPA hydroxyl radical is oxidized. It may have reduced the activity of the reaction, thereby reducing the efficiency of the degradation reactions [32].

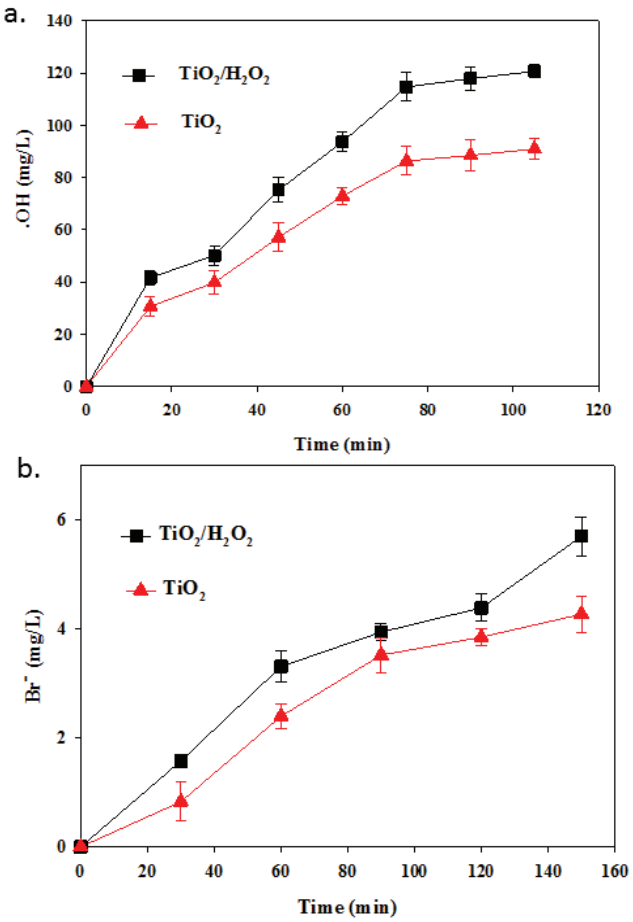


Fig. 4. The generation of hydroxyl radical (a) and bromide ions (b).

### 3.3. Degradation metabolism

Based on the previous conclusions, when $H_2O_2$ was added to 500°C-calcined $TiO_2$, the degradation rate significantly increased, while the 900°C-calcined $TiO_2$ degradation decreased. Thus, the degradation products of this article of the analytical process were chosen for the 500°C-calcined $TiO_2/H_2O_2$/UV combination to understand the details of hydroxyl radical formation, TBBPA debromination and specific types of degradation products derived through a specific degradation pathway or mechanism.

#### 3.3.1. Transformation of TBBPA and generation of ·OH

·OH is the core of the photocatalytic reaction and acts as an oxidizing agent to produce a hydroxyl radical of TBBPA after $TiO_2/H_2O_2$/UV irradiation. The degradation rate is directly affected by the level of its production, and the process of measuring the reaction generated. The ·OH concentration is particularly important. In this paper, a salicylic acid scavenger in the reaction of 2,5-DHBA was used to indirectly measure how many hydroxyl radicals were produced. Fig. 4(a) shows that in the $TiO_2$-only catalyst degradation experiments, TBBPA and the $TiO_2/H_2O_2$/UV combination of TBBPA degradation are relatively similar. In the first 75 min, the reaction rates are faster, with more 2,5-DHBA production, and after 75 min, the reaction rate begins to slow down. The $TiO_2/H_2O_2$ combined rates at each time point were higher than the yield only in the presence of $TiO_2$ under UV, which indirectly indicates that the $TiO_2/H_2O_2$/UV combination produces a relatively high yield of hydroxyl radicals. After 105 min, the $TiO_2/H_2O_2$/UV combination resulting in 2,5-DHBA was 120.70 mg/L (yield 78.4%), which was higher than the yield of $TiO_2$ 93.43 mg/L (60.7% yield), with a yield improvement of 29.2%. From the trend curve, it is obvious that hydroxyl radicals were produced within the first 75 min and gradually decreased after that. Researchers proposed that the reaction time would increase as the hydroxyl radicals further react with the degradation products [32–35].

Previous experimental results also showed that the degradation rate of TBBPA under various conditions rapidly increases with time before gradually slowing down and finally stabilizing. This conclusion is consistent with the trend curve of 2,5-DHBA, which indicates the amount of the reactants chosen to produce hydroxyl radicals must comply with this rule.

#### 3.3.2. Transformation of TBBPA and generation of $Br^-$

Although TBBPA is widely used for its high content of bromine atoms (58.9%), and the bromine atom source TBBPA is toxic, a measurement of the pathway of the reaction of the bromide ions may indirectly indicate the pros and cons regarding the yield of the reaction system to the TBBPA debromination

detoxification efficacy. Thus, in this experiment, only experiments detecting the bromide ion species were conducted for the $TiO_2$ catalyst degradation of TBBPA and the $TiO_2/H_2O_2$/UV combination for TBBPA degradation. The reaction rate from the $TiO_2/H_2O_2$/UV combination and the resulting rapid increase in the bromide ion content, can be seen in Fig. 4(b) within the first 90 min. Then, from 60 to 150 min, the reaction rate slows down, gradually approaching the maximum yield; the reactions of $TiO_2$ and $TiO_2/H_2O_2$/UV are similar to the reaction process at each time point, but the bromide ions generated by the former were lower than by the latter. $TiO_2/H_2O_2$/UV combination resulted in a bromide ion maximum yield of 4.23 mg/L (debromination rate: 71.8%) which is higher than the yield of $TiO_2$ of 3.78 mg/L (debromination rate: 64.2%), such that the debromination rate increased by 11.9%.

TBBPA has one of the highest bromine contents of all BFRs, which is the source of its toxicity. The purpose of TBBPA degradation is to remove bromine atoms, and then the benzene ring is eventually completely degraded by TBBPA via oxidation. Therefore, the bromine ion yield can indirectly indicate the performance of the TBBPA degradation system and its effective detoxification ability. The trend in the graph follows the requirements of this experiment, namely, to capture the hydroxyl radicals mentioned earlier. The reaction rate increases rapidly at first, then gradually slows down, and finally becomes stable. A higher final yield bromide ion, debromination of 71.8%, indicates that the $TiO_2/H_2O_2$/UV reaction system has obvious advantages in terms of the removal of bromide ion [36,37].

### 3.4. Degradation product and pathway of TBBPA removal by nano-$TiO_2$

The total number of ions and a time-varying curve was measured to obtain the various mass to charge ratios using mass spectrometry (Fig. S3). Components were measured by chromatography with a constant flow into the MS and mass scanning with continuous data collection. Each scan obtained a spectrum, and the ionic strength was determined by adding each spectrum to obtain the total ion current intensity. Then, ionic strength as the ordinate and time as the abscissa plotted to obtain the total ion chromatogram [38]. In this study, by detecting the $TiO_2/H_2O_2$/UV combination ion current degradation of TBBPA over different timeframes, the whole process of degradation, including intermediates, could be observed. As seen from Fig. 5, after the start of the reaction (from 10 to 150 min), TBBPA was largely degraded, indicating that the effect of the $TiO_2/H_2O_2$/UV combination on TBBPA can yield a relatively high degradation efficiency. In previous studies, the major degradation products are dibromo product of bisphenol A, bromine bisphenol A, bisphenol A, tribromophenol, dibromo phenol, and bromophenol [39].

The ion current determined from the spectrum analysis showed that in this reaction the degradation process produced five types of degradation products (Fig. S4). It can be concluded that TBBPA finally formed opened loop after the gradual debromination until the degradation of small molecules is eventually completed. In this study, four detected intermediates have been found in previous studies. 2,6-Dibromo-4-(2-hydroxypropan-2-yl)phenol, 2,6-dibromo-4-(hydroxymethyl)phenol,

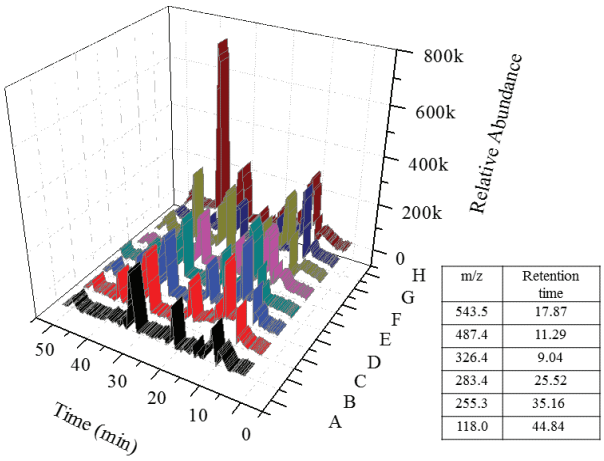


| m/z | Retention time |
|---|---|
| 543.5 | 17.87 |
| 487.4 | 11.29 |
| 326.4 | 9.04 |
| 283.4 | 25.52 |
| 255.3 | 35.16 |
| 118.0 | 44.84 |

Fig. 5. Total ion chromatogram of the degradation products at different sampling times: (A) 10 min; (B) 20 min; (C) 30 min; (D) 45 min; (E) 60 min; (F) 90 min; (G) 120 min; and (H) 150 min.

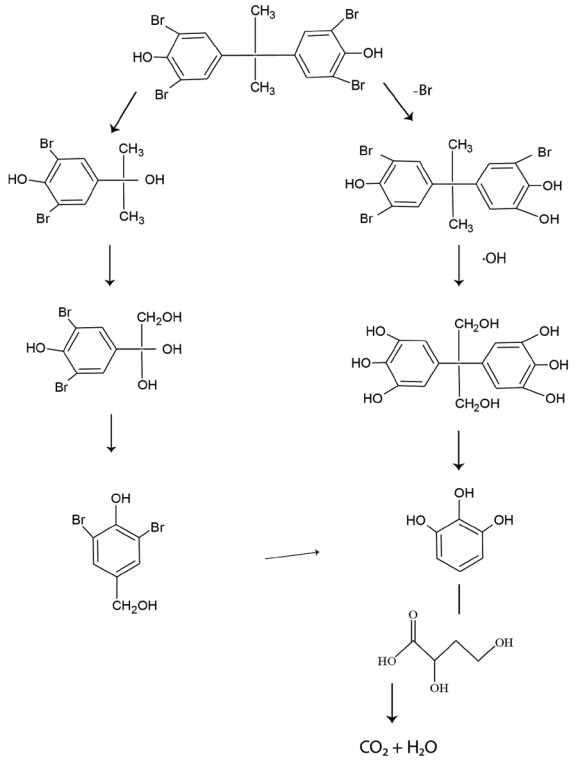


Fig. 6. The proposed degradation pathway of TBBPA.

2-(3,5-dibromo-4-hydroxyphenyl)-2-methylpropanoic acid, and 2,4-dihydroxybutanoic acid have been detected in another oxidation process in previous descriptions [40]. It is different from the oxidative process in the catalytic system comprised of iron(III)-tetrakis(*p*-sulfophenyl)porphyrin, $KHSO_5$, and humic acids [41]. The degradation pathway is mainly divided into two paths (Fig. 6). The first path is the degradation of

the benzene ring of TBBPA in one side, which is first oxidized open loop, then debrominated until a bromine phenol is formed. Ultimately, the open loop occurred. The other degradation pathway is the direct debromination of TBBPA based on the completion of bromine oxide ring opening, and eventually, which is completely degraded. The following is a detailed analysis of the degradation process. The results of this study are similar to those of previously described [42].

## 4. Conclusions

The combined $TiO_2/H_2O_2$/UV photocatalytic process was applied to treat TBBPA. The sol–gel method was used to produce different nano-$TiO_2$ powders at different temperatures (200°C–900°C in the interval of 100°C), XRD analysis revealed that 500°C-calcined samples show most effective degradation to TBBPA, which are mainly anatase $TiO_2$. The photocatalytic process in an aqueous system was optimized with UV (40–120 W) irradiation, $H_2O_2$ (1.5%–6.0%), and $TiO_2$ (100–500 mg/L). The degradation efficiency of TBBPA under optimal conditions (120 W UV, 3% $H_2O_2$, and 400 mg/L of 500°C-calcined $TiO_2$) was 99.3% after 150 min. Hydroxyl radicals (·OH) were the main reactive oxidative species involved in attacking TBBPA. Bromide ions increased with the conducting reaction. Five intermediates of TBBPA were detected by LC–MS, and a degrading pathway was proposed based on the products information.

## Acknowledgements

This work was supported in part by the Guangdong Province Scientific and Technological Project (2016A050503029), Fundamental Research Funds for the Universities (161gpy27), and the Research Fund Program of Guangdong Provincial Key Laboratory of Environmental Pollution Control and Remediation Technology (2016K0008).

## References

[1] S. Morris, C.R. Allchin, B.N. Zegers, J.J.H. Haftka, J.P. Boon, C. Belpaire, P.E.G. Leonards, S.P.J. van Leeuwen, J. de Boer, Distribution and fate of HBCD and TBBPA brominated flame retardants in North Sea Estuaries and aquatic food webs, Environ. Sci. Technol., 38 (2004) 5497–5504.
[2] S. Kitamura, N. Jinno, S. Ohta, H. Kuroki, N. Fujimoto, Thyroid hormonal activity of the flame retardants tetrabromobisphenol A and tetrachlorobisphenol A, Biochem. Biophys. Res. Commun., 293 (2002) 554–559.
[3] B. Ravit, J.G. Ehrenfeld, M.M. Häggblom, Salt marsh rhizosphere affects microbial transformation of the widespread halogenated contaminant tetrabromobisphenol-A (TBBPA), Soil Biol. Biochem., 37 (2005) 1049–1057.
[4] WHO, Tetrabromobisphenol A and Derivatives, International Program on Chemical Safety [R], Geneva, Switzerland, 1995.
[5] Y. Tada, T. Fujitani, N. Yano, H. Takahashi, K. Yuzawa, H. Ando, Y. Kubo, A. Nagasawa, A. Ogata, H. Kamimura, Effects of tetrabromobisphenol A, brominated flame retardant, in ICR mice after prenatal and postnatal exposure, Food Chem. Toxicol., 44 (2006) 1408–1413.
[6] M. Koizumi, Y. Yamamoto, Y. Ito, M. Takano, T. Enami, E. Kamata, R. Hasegawa, Comparative study of toxicity of 4-nitrophenol and 2,4-dinitrophenol in newborn and young rats, J. Toxicol. Sci., 26 (2001) 299–311.
[7] J.A. Szymanska, A. Sapota, B. Frydrych, The disposition and metabolism of tetrabromobisphenol-A after a single i.p. dose in the rat, Chemosphere, 45 (2001) 693–700.
[8] Y. Nakagawa, T. Suzuki, H. Ishii, A. Ogata, Biotransformation and cytotoxicity of a brominated flame retardant, tetrabromobisphenol A, and its analogues in rat hepatocytes, Xenobiotica, 37 (2007) 693–708.
[9] WHO, Environmental Health Criteria 172, Tetrabromobisphenol A and Derivative [S], Geneva, Switzerland, 1995.
[10] S. Pullen, R. Boecker, G. Tiegs, The flame retardants tetrabromobisphenol A and tetrabromobisphenol A-bisallylether suppress the induction of interleukin-2 receptor alpha chain (CD25) in murine splenocytes, Toxicology, 184 (2003) 11–22.
[11] H. Viberg, P. Eriksson, Differences in neonatal neurotoxicity of brominated flame retardants, PBDE 99 and TBBPA, in mice, Toxicology, 289 (2011) 59–65.
[12] T. Reistad, E. Mariussen, A. Ring, F. Fonnum, In vitro toxicity of tetrabromobisphenol-A on cerebellar granule cells: cell death, free radical formation, calcium influx and extracellular glutamate, Toxicol. Sci., 96 (2007) 268–278.
[13] H. Lilienthal, M.V. Cynthia, Exposure to tetrabromobisphenol A (TBBPA) in Wistar rats: neurobehavioral effects in offspring from a one-generation reproduction study, Toxicology, 246 (2008) 45–54.
[14] R.V. Kuiper, E.J. van den Brandhof, P.E. Leonards, L.T. van der Ven, P.W. Wester, J.G. Vos, Toxicity of tetrabromobisphenol A (TBBPA) in zebrafish (Danio rerio) in a partial life-cycle test, Arch. Toxicol., 81 (2007) 1–9.
[15] N. Fujimoto, S. Maruyama, A. Ito, Establishment of an estrogen responsive rat pituitary cell subline MtT/E-2, Endocr. J., 46 (1999) 389–396.
[16] J.G. Hollowell Jr., P.L. Garbe, D.T. Miller, Maternal thyroid deficiency during pregnancy and subsequent neuropsychological development of the child, N. Engl. J. Med., 341 (1999) 549–555.
[17] M. Grabda, S. Oleszek-Kudlak, M. Rzyman, E. Shibata, T. Nakamura, Studies on bromination and evaporation of zinc oxide during thermal treatment with TBBPA, Environ. Sci. Technol., 43 (2009) 1205–1210.
[18] M. Grabda, S. Oleszek-Kudlak, E. Shibata, T. Nakamura, Influence of temperature and heating time on bromination of zinc oxide during thermal treatment with tetrabromobisphenol A, Environ. Sci. Technol., 43 (2009) 8936–8941.
[19] M. Rzyman, M. Grabda, S. Oleszek-Kudlak, E. Shibata, T. Nakamura, Studies on bromination and evaporation of antimony oxide during thermal treatment of tetrabromobisphenol A (TBBPA), J. Anal. Appl. Pyrolysis, 88 (2010) 14–21.
[20] E. Shibata, M. Grabda, T. Nakamura, Thermodynamic consideration of the bromination reactions of inorganic compounds, J. Jpn. Soc. Waste Manage. Experts, 17 (2006) 361–371.
[21] Q. Zhu, M. Igarashi, M. Sasaki, T. Miyamoto, R. Kodama, M. Fukushima, Degradation and debromination of bromophenols using a free-base porphyrin and metalloporphyrins as photosensitizers under conditions of visible light irradiation in the absence and presence of humic substances, Appl. Catal., B, 183 (2016) 61–68.
[22] K. Lin, W. Liu, J. Gan, Reaction of tetrabromobisphenol A (TBBPA) with manganese dioxide: kinetics, products, and pathways, Environ. Sci. Technol., 43 (2009) 4480–4486.
[23] T. Peng, D. Zhao, K. Dai, W. Shi, K. Hirao, Synthesis of titanium dioxide nanoparticles with mesoporous anatase wall and high photocatalytic activity, J. Phys. Chem., 109 (2005) 4947–4952.
[24] S.M. Klein, V.N. Manoharan, D.J. Pine, F.F. Lange, Synthesis of spherical polymer and titania photonic crystallites, Langmuir, 21 (2005) 6669–6674.
[25] H. Shibata, H. Mihara, T. Mukai, T. Ogura, H. Kohno, T. Ohkubo, H. Sakai, M. Abe, Preparation and formation mechanism of mesoporous titania particles having crystalline wall, Chem. Mater., 18 (2006) 2256–2260.
[26] M. Addamo, V. Augugliaro, A.D. Paola, E. García-López, V. Loddo, G. Marc, R. Molinari, L. Palmisano, M.S. Preparation, Characterization and photoactivity of polycrystalline nanostructured $TiO_2$ catalysts, Phys. Chem. B., 108 (2004) 3303–3310.

[27] C. Krüger, Polybrominated Biphenyls and Polybrominated Diphenyl Ethers – Detection and Quantitation in Selected Foods [D], PhD Thesis, University of Munster, Germany, 1988 (in German).
[28] S.H. Wang, E. Raptis, J. Yeh, Ion chromatography for the determination of sulfate in STEALTH® liposomes, J. Chromatogr., A, 1039 (2004) 51–58.
[29] A.Y. Ahmed, T.A. Kandiel, T. Oekermann, D. Bahnemann, Photocatalytic activities of different well-defined single crystal $TiO_2$ surfaces: anatase versus rutile, J. Phys. Chem. Lett., 2 (2011) 2461–2465.
[30] J. Jia, S. Zhang, P. Wang, H. Wang, Degradation of high concentration 2,4-dichlorophenol by simultaneous photocatalytic–enzymatic process using $TiO_2$/UV and laccase, J. Hazard. Mater., 205–206 (2012) 150–155.
[31] E.S. Elmolla, M. Chaudhuri, Photocatalytic degradation of amoxicillin, ampicillin and cloxacillin antibiotics in aqueous solution using UV/$TiO_2$ and UV/$H_2O_2$/$TiO_2$ photocatalysis, Desalination, 252 (2010) 46–52.
[32] P. Konieczka, J. Namieśnik, Estimating uncertainty in analytical procedures based on chromatographic techniques, J. Chromatogr., A, 1217 (2010) 882–891.
[33] P. Westerhoff, S.P. Mezyk, W.J. Cooper, D. Minakata, Electron pulse radiolysis determination of hydroxyl radical rate constants with Suwannee River fulvic acid and other dissolved organic matter isolates, Environ. Sci. Technol., 41 (2007), 4640–4646.
[34] B. Halliwell, H. Kaur, M. Ingelman-Sundbergm, Hydroxylation of salicylate as an assay for hydroxyl radicals: a cautionary note, Free Radical Biol. Med., 10 (1991) 439–441.
[35] Z. Maskos, J.D. Rush, W.H. Koppenol, The hydroxylations of phenylalanine and tyrosine are similar to that of salicylate, Free Radical Biol. Med., 8 (1990) 153–162.
[36] M.E. Lindsey, M.A. Tarr, Quantitation of hydroxyl radical during Fenton oxidation following a single addition of iron and peroxide, Chemosphere, 41 (2000) 409–417.
[37] J.W. Voordeckers, D.E. Fennell, K. Jones, M.M. Häggblom, Anaerobic biotransformation of tetrabromobisphenol A, tetrachlorobisphenol A, and bisphenol A in estuarine sediments, Environ. Sci. Technol., 36 (2002) 696–701.
[38] N. Schneider, K. Werkmeister, M. Pischetsrieder, Analysis of nisin A, nisin Z and their degradation products by LCMS/MS, Food Chem., 127 (2011) 847–854.
[39] C.I.T. Institute, Biodegradation and Bioaccumulation Date of Existing Chemicals Based on the CSCL Japan, Tokyo Toxiclogy and Information Center, Japan Chemical Industry Ecology, Japan, 1992.
[40] Y. Ding, L. Zhu, N. Wang, H. Tang, Sulfate radicals induced degradation of tetrabromobisphenol A with nanoscaled magnetic $CuFe_2O_4$ as a heterogeneous catalyst of peroxymonosulfate, Appl. Catal., B, 129 (2013) 153–162
[41] M. Fukushima, Y. Ishida, S. Shigematsu, H. Kuramitz, S. Nagao, Pattern of oxidation products derived from tetrabromobisphenol A in a catalytic system comprised of iron(III)-tetrakis(*p*-sulfophenyl)porphyrin, $KHSO_5$ and humic acids, Chemosphere, 80 (2010) 860–865
[42] Y. Guo, X. Lou, D. Xiao, L. Xu, Z. Wang, J. Liu, Sequential reduction–oxidation for photocatalytic degradation of tetrabromobisphenol A: kinetics and intermediates, J. Hazard. Mater., 241–242 (2012) 301–306.
[43] R.A. French, A.R. Jacobson, B. Kim, S.L. Isley, R.L. Penn, P.C. Baveye, Influence of ionic strength, pH, and cation valence on aggregation kinetics of titanium dioxide nanoparticles, Environ. Sci. Technol., 43 (2009) 1354–1359.
[44] S. Horikoshi, T. Miura, M. Kajitani, Photodegradation of tetrahalobisphenol-A (X=Cl, Br) flame retardants and delineation of factors affecting the process, Appl. Catal., B, 84 (2008) 797–802.
[45] K. Hashimoto, H. Irie, A. Fujishima, $TiO_2$ photocatalysis: a historical overview and future prospects, Jpn. J. Appl. Phys., Part 1, 44 (2005) 8269–8285.
[46] A. Fujishima, K. Hashimoto, T. Watanabe, $TiO_2$ Photocatalysis Fundamentals and Applications, BKC Publication, Tokyo, 1999.

# Supplementary information

**1. Influence by $SO_4^{2-}$**

Sulphate ion effect on the catalytic process by the $TiO_2$ [43]. They are mainly from the preparation process to produce effective nano-$TiO_2$ catalysts and other raw materials and the tetrabromobisphenol A (TBBPA) wastewater [44]. The influence of sulphate ions on $TiO_2$ for the 500°C treatment is reflected in the last 30 min, a lower degradation rate occurs for each period, and the overall presentation indicates inhibited degradation reactions (Fig. S2(a)). However, inhibition from the sulphate ions on the performance of the 900°C treated $TiO_2$ was not significant (Fig. S2(b)); the degradation efficiency of each period is more consistent, which may be a result of sulphate ion bonds reducing the agglomeration of the catalyst, increasing its suspension properties in solution [45,46]. To study the effects of sulphate ions on the TBBPA degradation efficiency in a $TiO_2/H_2O_2$/UV combined process, this experiment was selected, monitored, and treated at different sulphate concentrations and reaction conditions to determine the 500°C–900°C nano-$TiO_2$ TBBPA degradation effectiveness. Fig. 3(c) clearly shows that the influence of sulphate ions on $TiO_2$ for the 500°C treatment is reflected in the last 30 min, a lower degradation rate occurs for each period, and the overall presentation indicates inhibited degradation reactions. However, inhibition from the sulphate ions on the performance of the 900°C-treated $TiO_2$ was not significant (Fig. 3(d)); the degradation efficiency of each period is more consistent, which may be a result of sulphate ion bonds reducing the agglomeration of the catalyst, increasing its suspension properties in solution, such that it has a more uniform contact with the reactants. Different concentrations of sulphuric acid are calculated to determine the presence of the $TiO_2$ degradation TBBPA maximum degradation rate, and we find different concentrations of sulphate ions for 500°C $TiO_2$ photocatalytic inhibition because the TBBPA degradation rate increases with the concentration of sulphate. The results show first an increasing trend and then a decreasing trend in 1.0 mg/L when the maximum degradation rate reached 63%, indicating that the concentration of sulphate had a minimal impact; the degradation rate of 0.1 mg/L at 51.7% is a minimum; and the effect of sulphate is maximized. It also shows the impact of the sulphate ions on 500°C $TiO_2/H_2O_2$ in which the sulphate concentration is increased after it first decreases. The sulphate for the 900°C $TiO_2$ photocatalytic properties plays a role in promoting the TBBPA degradation rate, in which it increased with increasing concentration of sulphate and then showed a decreasing trend. Likewise, it also shows that sulphate ions in 900°C $TiO_2/H_2O_2$ have an effect. The sulphate concentration is increased after it first decreases. At 1.5 mg/L, the maximum degradation rate is 77.2%, the largest role in promoting the degradation rate can be seen for 2.0 mg/L at a 58.8% minimum.

**2. Degradation kinetics**

In the $TiO_2/H_2O_2$/UV combination for TBBPA degradation experiments, LC–MS was applied to analyze the degradation products and proposed degrading pathway. Total ion chromatogram sampling at different times and the intermediate mass spectrum are shown in Figs. S3 and S4, respectively.

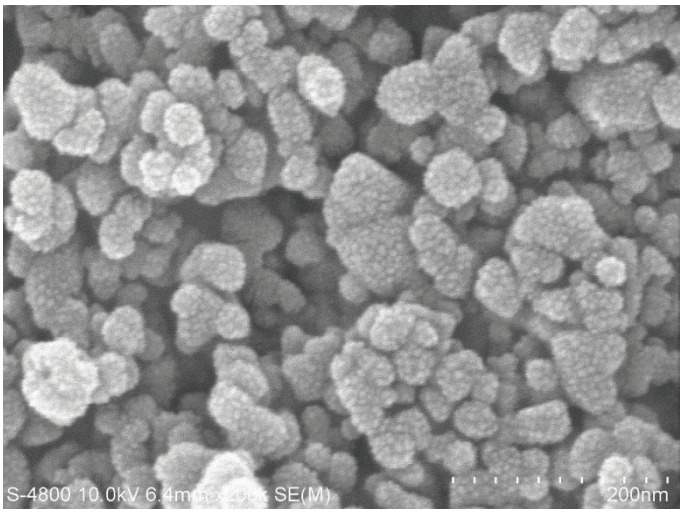


Fig. S1. SEM image of nano-$TiO_2$.

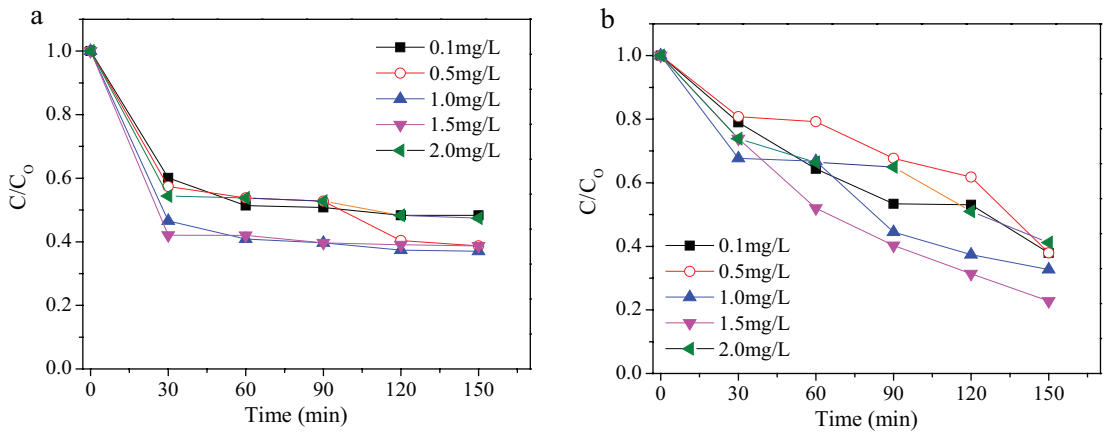


Fig. S2. Degradation of TBBPA by UV/$TiO_2$/$H_2O_2$ process influenced by different concentrations of $SO_4^{2-}$ ((a) 500°C $TiO_2$ and (b) 900°C $TiO_2$).

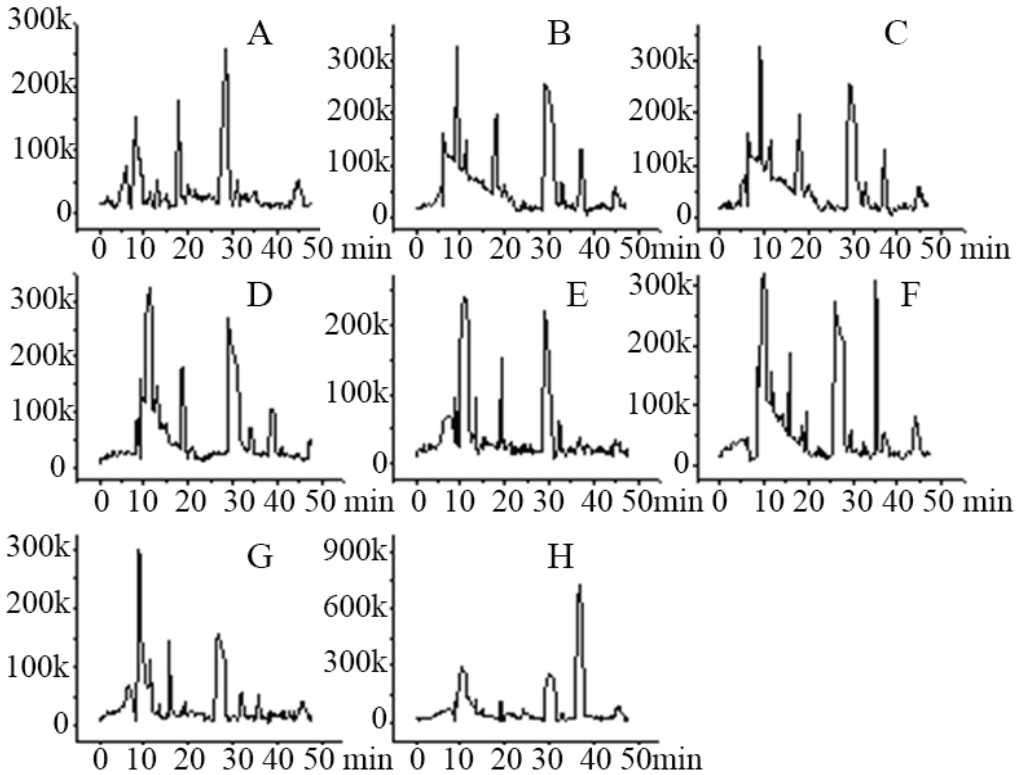


Fig. S3. Total ion chromatogram of the TBBPA products sampling at different times: (A) 10 min; (B) 20 min; (C) 30 min; (D) 45 min; (E) 60 min; (F) 90 min; (G) 120 min; and (H) 150 min.

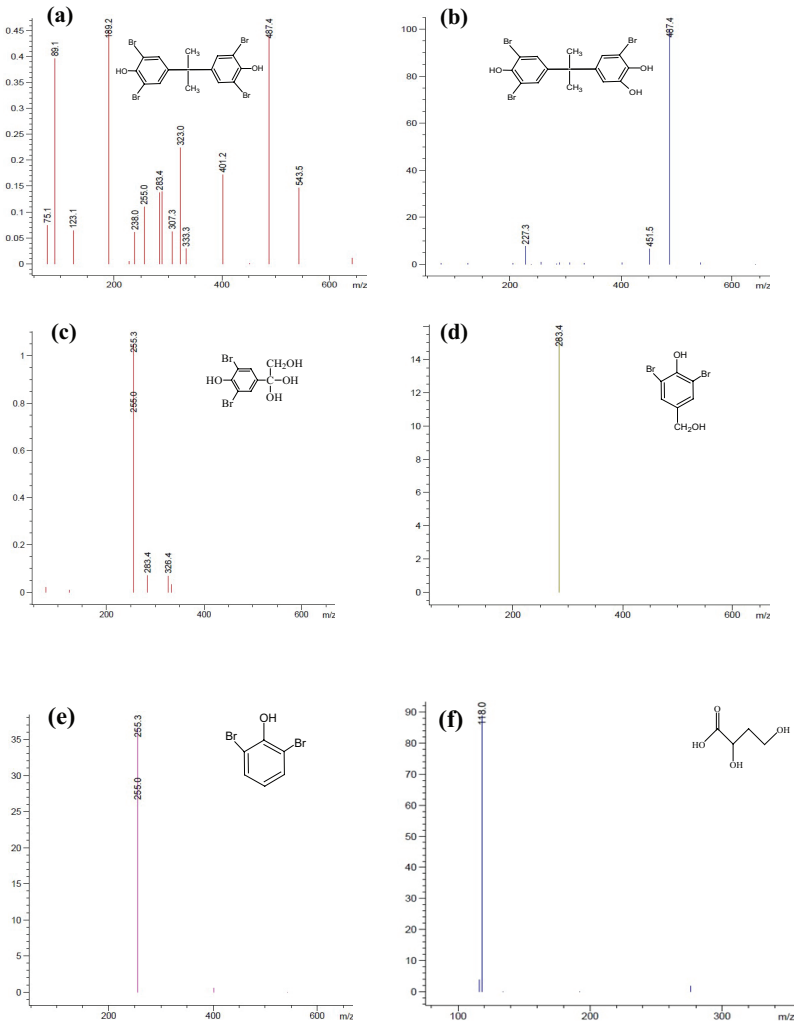


Fig. S4. The mass spectrum of degradation product.